JGR Oceans

RESEARCH ARTICLE

10.1029/2025JC022556

Phytoplankton Bloom Changes During Three Regime Shifts Derived From Sea Ice Concentration in the Ross Sea

Hyun-Jin Yang[1,2], Dukwon Bae[3], Jinku Park[4], Hyun-Cheol Kim[5], Federico Ienna[6], and Young-Heon Jo[1,2,7]

[1]BK21 School of Earth Environmental Systems, Pusan National University, Busan, Republic of Korea, [2]Department of Oceanography, Pusan National University, Busan, Republic of Korea, [3]Department of Civil, Urban, Earth, and Environmental, Ulsan National Institute of Science and Technology (UNIST), Ulsan, Republic of Korea, [4]Center of Remote Sensing & GIS, Korea Polar Research Institute, Incheon, Republic of Korea, [5]Division of Ocean & Atmosphere Sciences, Korea Polar Research Institute, Incheon, Republic of Korea, [6]Istituto Nazionale di Oceanografia e di Geofisica Sperimentale (OGS), Sgonico, Italy, [7]Marine Research Institute, Pusan National University, Busan, Republic of Korea

Abstract Sea Ice Concentration (SIC) plays an important role in the Antarctic polynyas, especially where biological interactions through changes in chlorophyll-a concentration (CHL) phenology are concerned. To specifically understand how much SIC change affects CHL in the Ross Sea polynya (RSP), the regime shift index (RSI) was applied to the SIC anomaly, as per Rudionov (2004), https://doi.org/10.1029/2004gl019448. This resulted in three principal temporal regimes: Regime 1 (R1), 1997–2004; Regime 2 (R2), 2004–2016; and Regime 3 (R3), 2016–2019. Based on reconstructed daily CHL observations from remote sensing and application of a random forest algorithm with 10 physical predictors, our analysis revealed that (a) earlier sea ice melt onset corresponds to an earlier CHL peak across all regimes; (b) SIC changes explain approximately 10%–12.5% of CHL variation in the RSP: a first-ever estimation of SIC influence in the RSP; and (c) although CHL is significantly influenced by SIC changes, the relative contributions of the 10 geophysical predictors vary across the three regimes, with photosynthetically active radiation consistently emerging as the dominant driver. This result may explain why CHL has been observed to decrease despite the unprecedented decrease in Antarctic SIC since 2016.

Plain Language Summary Sea Ice Concentration strongly influences Antarctic polynyas, where open water surrounded by sea ice supports high biological productivity. In the RSP, changes in sea ice affect the timing and strength of phytoplankton blooms, which are commonly tracked using chlorophyll-a concentration. However, the extent to which sea ice changes directly controls variability in chlorophyll-a concentration has not been well quantified. In this study, we examined how chlorophyll-a changed over time by dividing recent decades into three periods based on sea ice conditions: an early period with high sea ice (1997–2004), a middle period with moderate sea ice (2004–2016), and a recent period with low sea ice (2016–2019). Using satellite observations and a machine-learning approach, we found that earlier sea ice melt is consistently associated with earlier phytoplankton bloom timing. Sea ice changes account for approximately 10%–12.5% of the variability in chlorophyll-a concentration, providing the first quantitative estimate of sea ice influence in this region. Other environmental factors, especially light availability, play an even larger role. This helps explain why chlorophyll levels have decreased in recent years despite strong reductions in Antarctic sea ice.

Key Points:

- Chlorophyll-a concentration (CHL) was estimated based on a Random Forest model for three periods of Sea Ice Concentration (SIC) change
- SIC changes explain approximately 10%–12.5% of CHL variation, which is the first ever estimation made for Ross Sea polynya
- Although SIC changes significantly influence CHL, 10 other geophysical predictors of CHL were found to be more dominant in each period

Supporting Information:

Supporting Information may be found in the online version of this article.

Correspondence to:

Y.-H. Jo,
joyoung@pusan.ac.kr

Citation:

Yang, H.-J., Bae, D., Park, J., Kim, H.-C., Ienna, F., & Jo, Y.-H. (2026). Phytoplankton bloom changes during three regime shifts derived from sea ice concentration in the Ross Sea. *Journal of Geophysical Research: Oceans*, *131*, e2025JC022556. https://doi.org/10.1029/2025JC022556

Received 26 FEB 2025
Accepted 14 FEB 2026

Author Contributions:

Conceptualization: Young-Heon Jo
Data curation: Dukwon Bae
Formal analysis: Hyun-Jin Yang, Jinku Park, Young-Heon Jo
Funding acquisition: Young-Heon Jo
Investigation: Jinku Park, Hyun-Cheol Kim
Methodology: Hyun-Jin Yang, Dukwon Bae
Project administration: Young-Heon Jo
Resources: Dukwon Bae, Hyun-Cheol Kim
Software: Hyun-Jin Yang, Jinku Park, Hyun-Cheol Kim

1. Introduction

The Ross Sea is the region where the largest polynya formation occurs in Antarctica, known as the Ross Sea polynya (RSP), which supports exceptionally high phytoplankton biomass (Arrigo & van Dijken, 2003b; Li et al., 2016). The RSP is the most productive area along with the Amundsen Sea polynya, with its annual primary productivity exceeding 150 g C m^{-2} (Arrigo & van Dijken, 2003b). Variations in SIC are closely linked to polynya formation, which promotes phytoplankton blooms during the austral summer. This occurs through enhanced nutrient upwelling (Jena & Pillai, 2020), modulation of light availability as thinning or retreating sea ice alters the penetration of solar radiation into the ocean surface (Assmy et al., 2017), and changes in mixed-layer thickness driven by meltwater injection during SIC advance and retreat (Li et al., 2016; Salmon et al., 2020; Soja-Woźniak et al., 2025). These phytoplankton bloom responses are detected by satellite and in situ measurements of chlorophyll-a concentration, a widely used proxy for phytoplankton biomass. Understanding these mechanisms is

Supervision: Young-Heon Jo
Validation: Hyun-Jin Yang, Jinku Park, Hyun-Cheol Kim
Visualization: Federico Ienna
Writing – original draft: Hyun-Jin Yang
Writing – review & editing: Hyun-Jin Yang, Federico Ienna, Young-Heon Jo

particularly important because variations in phytoplankton biomass directly influence the abundance and reproductive success of higher trophic-level organisms in the RSP by affecting food availability and energy transfer within the marine ecosystem (Comiso et al., 2011; Massom & Stammerjohn, 2010; Park et al., 2018; Saenz & Arrigo, 2014). However, few quantitative studies to date have estimated the extent to which SIC and other physical forces contribute to phytoplankton blooms in this region.

Over the last 40 yrs, Antarctic sea ice extent has increased significantly, particularly in the Ross Sea (Comiso et al., 2011; Parkinson, 2019; Yuan et al., 2017). However, between 2015 and 2020, Antarctic sea ice extent recorded an unprecedented decline, losing in 3 yrs an area comparable to that which the Arctic lost over three decades (Parkinson & DiGirolamo, 2021). The Ross Sea, the study area, experienced its lowest sea ice extent in February 2017, leading to a distinct shift in sea ice conditions after 2016 (Parkinson, 2019). This reversal may impact marine ecosystems in the Antarctic Ocean (Turner et al., 2017), for example, krill (Atkinson et al., 2004), and emperor penguins (Fretwell et al., 2023). Despite the strong negative correlation between SIC and chlorophyll-a concentration ($R = -0.84$, $p < 0.05$; Chen & Meng, 2022), both phytoplankton bloom extent and chlorophyll-a concentration have declined sharply since the unprecedented retreat of SIC in 2016.

Conducting research at high latitudes is highly challenging due to limited access to extreme environments. Therefore, many researchers have used satellite observations and limited field measurements (Portela et al., 2025; Thomalla et al., 2023). Because SIC can be measured by microwave remote sensing, it is unaffected by weather conditions, unlike ocean color remote sensing used for chlorophyll-a concentration measurements. To determine missing values in spatiotemporal chlorophyll-a concentration data sets, several studies have used machine learning-based interpolated data, among other methods (Park et al., 2020; Zhan et al., 2017). Figure 1 shows the total percentage of regions with unavailable satellite ocean color chlorophyll-a concentrations (CHL_{SAT}) due to cloud cover during the study period from 1 September 1997–28 February 2019. The availability of CHL_{SAT} varies spatially, with virtually no observations in offshore regions and along ice shelves, increasing to approximately 30% coverage in Terra Nova Bay and the RSP. Due to limitations imposed by cloud cover, seasonal variability in chlorophyll-a concentration has primarily been investigated using monthly CHL_{SAT} data (Turner et al., 2025). In this study, we use reconstructed daily chlorophyll-a concentration derived from ensemble-based machine learning to overcome temporal constraints, enabling a more precise analysis of bloom phenology in the Ross Sea, given the brief duration and subtle variability of bloom-related signals.

In this study, we analyze the decreasing chlorophyll-a concentration in response to the unprecedented retreat of SIC in the Ross Sea since 2016, as well as the impact of other physical variables. Accordingly, three important results are addressed: (a) whether the low ice period from 2016 to 2020 is defined as a regime shift. The performance of the random forest (RF) model for reconstructing chlorophyll-a concentration, Section 3.1; (b) chlorophyll-a concentration response to shifts in SIC regimes, in Section 3.2, and 3 contributions of SIC and other geophysical drivers to chlorophyll-a concentration variability in the three regimes, in Section 3.3.

2. Data and Methods

The two primary methodologies employed in this study are regime shift detection and the RF method. Regime shift detection was used to classify periods based on the SIC anomaly (SICA). In contrast, RF modeling, a machine learning technique, was used to predict chlorophyll-a concentration variability with physical predictors. Notably, SIC was excluded as a direct input variable in the RF model due to its distinct physical domain compared to the other 10 predictors. In particular, SIC values tend to be near zero in regions where phytoplankton blooms occur, unlike other physical variables. For example, when CHL_{SAT} exceeds 1 mg m^{-3}, 88.06% of the data points have SIC below 10%, and 41.23% have SIC below 1%. This asymmetric distribution means that SIC is not suitable as an input for RF training. Instead, we assessed the influence of SIC separately through regime-based analysis of chlorophyll-a concentration phenology. Additionally, SIC was applied as a masking index to exclude areas with SIC >60%, where CHL_{SAT} cannot be reliably observed (Park et al., 2020).

Phytoplankton dynamics in the Ross Sea may be influenced by a range of physical and environmental factors, including sea ice, temperature, wind, nutrients, light availability, mixed layer depth (MLD), and stratification (Arrigo & van Dijken, 2004; Behera et al., 2020; Park et al., 2019; Sokolov, 2008). Accordingly, regime shift detection was used to separate periods based on sea ice distribution. Sea surface temperature (SST) and 2-m air temperature (T2M), which are associated with thermal forcing such as heat flux, 10-m zonal and meridional winds (U10 and V10), which can influence sea ice movement, vertical mixing, and upwelling processes that supply

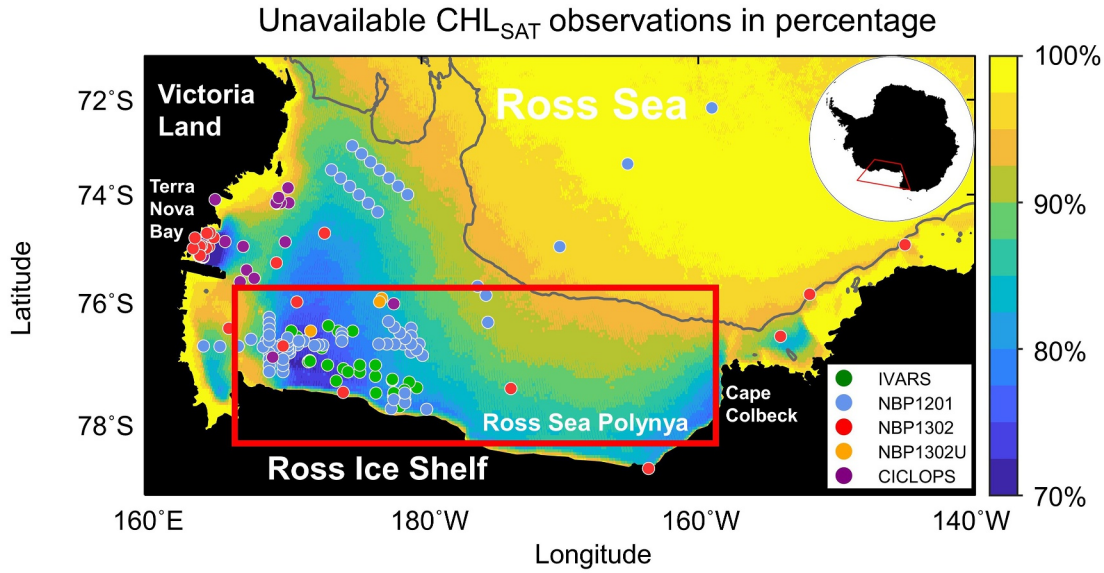

Figure 1. Unavailability of satellite ocean color chlorophyll-a concentration (CHL_{SAT}) observations by percentage during the austral spring to summer (November–February). The black contour line at 1200 m depth indicates the division between the continental shelf area (the main study area) and the open ocean. The circles illustrate the in situ measurement data from the five cruises: IVARS (green), NBP1201 (sky-blue), NBP1302 (red), NBP1302U (yellow), and CICLOPS (purple). The red box highlights the Ross Sea polynya.

nutrients to the surface layer, and photosynthetically active radiation (PAR), which directly affects phytoplankton photosynthesis, were selected as input variables to the RF model (category (2) in Table 1). However, MLD often exhibits substantial biases in the Antarctic due to limited observations (Sallée et al., 2013; Treguier et al., 2023). Accordingly, wind variables were used as proxies rather than directly incorporating model-based MLD. In addition, to mitigate the influence of physical factors not explicitly represented, including MLD, longitude (LON), latitude (LAT), day of year (DOY), bathymetry (DEP), and climatology of chlorophyll-a concentration (CHL_{CLIM}) were included as variables used as contextual features to help the model learn spatial and seasonal patterns (Category (3) in Table 1). Such variables are commonly used in remote sensing–based chlorophyll concentration prediction studies (Clay et al., 2019; Park et al., 2020). All selected variables were used as inputs to

Table 1
Nomenclature, Range, Resolution, and Data Source of the Ten Predictor Variables Used in the Random Forest (RF) Model to Reconstruct Chlorophyll-A Concentration

Category	Variable name	Abbreviation	Range (unit)	Ordinary resolution	Source	Data origin
(1)	Sea ice concentration	SIC	0 to 100 (%)	10 km	OSISAF	*S*
(2)	Sea surface temperature	SST	−1.8 to 3.706 (℃)	25 km	OISST	*R*
	Photosynthetically active radiation	PAR	0 to 161.519 (W m^{-2})	25 km	ERA-interim	*R*
	2 m atmospheric temperature	T2M	208.711 to 278.643 (K)	25 km		
	10 m zonal wind	U10	−28.122 to 27.999 (m s^{-1})	25 km		
	10 m meridional wind	V10	−27.355 to 34.832 (m s^{-1})	25 km		
(3)	Longitude	LON	160 (°E) to 140 (°W)	4 km		
	Latitude	LAT	79 to 70 (°S)	4 km		
	Day of year	DOY	305 (1 November) to 59 (28 February)			
	Bathymetry	DEP	−5,075 to 3,356 (m)	~1 km	GEBCO	
	Climatology of chlorophyll-a concentration	CHL_{CLIM}	0.03 to 5.5 (mg m^{-3})	4 km	Globcolour	*S*
(4)	Satellite chlorophyll-a concentration	CHL_{SAT}	0.003 to 92.211 (mg m^{-3})	4 km	Globcolour	*S*

Note. *S* and *R* denote satellite-derived and reanalysis data, respectively. Variables are categorized according to their use: (1) variables used in the regime shift detection method to reconstruct daily fields of chlorophyll-a concentration, (2) input for the RF model, (3) variables used as contextual features to help the model learn spatial and seasonal patterns, and (4) output from the RF model. SIC was not used for model input, but for regime shift detection.

the RF model to generate gap-free, daily reconstructed chlorophyll-a concentration (CHL_{REC}). Because the input data sets have different spatial resolutions, bilinear interpolation was used to place the target data onto the grid.

2.1. Regime Shift Detection From SICA Time Series

Sea Ice Concentration data were obtained from the European Organization for the Exploitation of Meteorological Satellites (EUMETSAT) Ocean and Sea Ice Satellite Application Facility (OSI SAF) (OSI SAF, 2022). Sea Ice Concentration was used to detect regime shifts and assess their influence on chlorophyll-a concentration variability. A decline in sea ice extent has been observed since 2016, indicating a possible regime shift in the Ross Sea and changes in the environmental factors affecting chlorophyll-a concentration. To detect regime shifts, we employed the regime shift index (RSI) to spatially average monthly SICA from November 1978 to February 2019 (Rodionov, 2004).

To compute the RSI, the cutoff length l (year) was set to define the initial continuous segment of the time series, representing the first regime (R1). The mean value of variable X over this R1 period is denoted as $\overline{X}_{R1}$. For each subsequent observation beginning at $i = l + 1$, the regime is evaluated by testing whether the x_i falls outside the range $\overline{X}_{R1} \pm \text{diff}$. The parameter diff represents the statistically significant difference between the mean states of two successive regimes, determined using the student's t-test.

$$\text{diff} = t\sqrt{2\sigma_l^2/l} \tag{1}$$

where t is the value from the t-distribution with $2l - 2$ degrees of freedom and σ_l^2 represents the variance of a l-year sliding window. A probability level of $p = 0.05$ was used. If the new observation x_i remains within $\overline{X}_{R1} \pm \text{diff}$, the current regime persists and $\overline{X}_{R1}$ is updated using the latest l observations. If x_i falls outside this range, the year is identified as a possible starting point j for a new regime ($R2$).

Once the shift point j is determined, each subsequent observation x_i for $i > j$ is tested against the null hypothesis of no regime shift at year j. If the anomaly $x_i - \overline{x}'_{R2}$ has the same sign as the anomaly at the shift point, the confidence in a true regime transition increases. Conversely, if the sign differs, the confidence decreases. These changes in confidence regarding the regime shift are reflected in the RSI, which is defined as the cumulative sum of normalized anomalies:

$$\text{RSI}_{i,j} = \sum_{i=j}^{j+m} \frac{x_i^*}{l\sigma_l}, m = 0, 1, \ldots, l-1 \tag{2}$$

For an upward transition, the adjusted anomaly is $x_i^* = x_i - \overline{x}'_{R2}$; for a downward transition, it is $x_i^* = \overline{x}'_{R2} - x_i$. Sustained positive (negative) RSI values throughout the l-year window indicate a statistically significant upward (downward) shift, respectively. We evaluated cutoff lengths l ranging from one to 10 yrs (Figure S1 in Supporting Information S1). Values below 4 yrs yielded weak or non-significant detections, whereas cutoffs of five to 9 yrs consistently identified the same shift timing. Accordingly, we selected a 5-year cutoff for our final RSI analysis, balancing robust statistical significance with sensitivity to interannual variability, which is significant at the 0.05 confidence level.

2.2. Reconstructing Chlorophyll-A Concentration Using RF Models

RF modeling is an algorithm based on decision trees in which model predictions are derived by averaging the results of multiple decision trees (Breiman, 2001). This machine learning technique works by "training" the algorithm through each decision tree recursion by selecting a subset of samples through bootstrap aggregation (bagging), which allows duplication in a given training set. Consequently, the ensemble mean (regression) of the training result is found at the end of the tree. A schematic diagram illustrating a simple concept of RF is shown in Figure 2. For data sets that include abnormal values near the edge of the cloud in the original data, as is typical of CHL_{SAT} data sets, the RF bagging technique is very well suited and reduces the error during the regression process (Park et al., 2020).

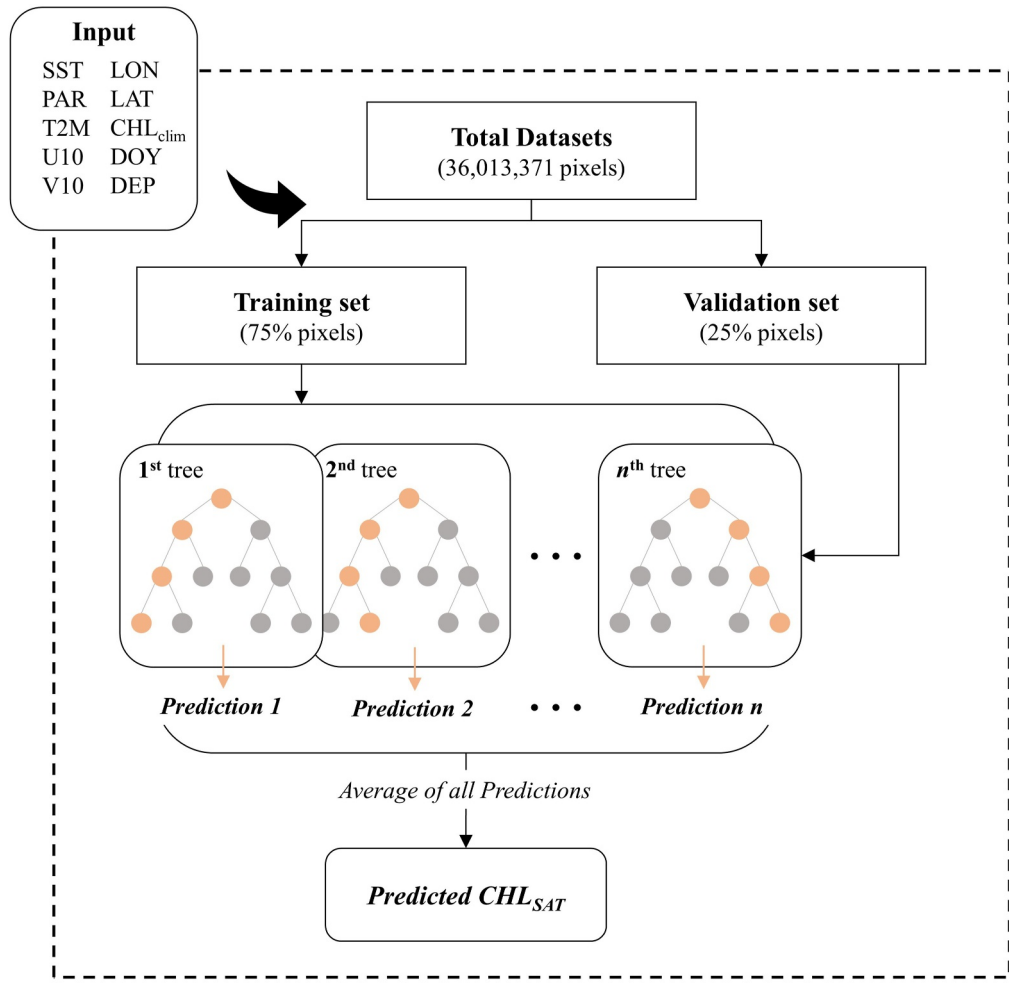

Figure 2. Schematic diagram of the random forest (RF) used for chlorophyll-a concentration reconstruction. Ten variables including Sea surface temperature, photosynthetically active radiation, 2 m atmospheric temperature (T2M), 10 m zonal wind (U10), 10 m meridional wind (V10), longitude (LON), latitude (LAT), climatology of chlorophyll-a concentration (CHL_{CLIM}), day of year, and bathymetry (DEP) were used as inputs, with CHL_{SAT} as the output.

CHL_{SAT} was used as the target data from 1 September 1997–28 February 2019. CHL_{SAT} has a spatial resolution of 4 km and consists of a weighted average of level 2 chlorophyll-a concentration products derived from various ocean color satellite sensors, such as the Sea-viewing Wide Field-of-view Sensor (SeaWiFS), the Moderate Resolution Imaging Spectroradiometer (MODIS), the Medium Resolution Imaging Spectrometer (MERIS), and Visible Infrared Imaging Radiometer Suite (VIIRS) (Maritorena et al., 2010; Maritorena & Siegel, 2005; O'Reilly et al., 2000). CHL_{SAT} data were obtained from the chlorophyll-a concentration 1 product (version 2018.4) of the European Space Agency's GlobColor Project (http://globcolour.info), which is suitable for Case-1 waters. Chlorophyll-a concentration 1 product includes the Garver-Siegel-Maritorena (GSM) and the averaged weighted (AVW) (GSM) merged models.

Other input variables for RF include SST data, which were obtained from version two of the NOAA daily optimum interpolation SST (Huang et al., 2021). Sea surface temperature was interpolated to a 4×4 km resolution, similar to the Globcolour CHL_{SAT} grid, through bilinear interpolation. In the Ross Sea, the freezing point was considered approximately −1.8°C or lower; any temperature value below this was considered to be SIC and was masked out. Global coverage of elevation data was obtained from the General Bathymetric Chart of the Ocean (GEBCO) on a 15 arc-second grid (GEBCO Compilation Group, 2019; https://www.gebco.net). The General Bathymetric Chart of the Ocean data were also used as bathymetric predictors.

Table 2
Summary of In Situ Data Sets Used for Validation, Including Sample Type and Date

	Project	Sample type	Abbreviation	Date	Data set ID
1	Smith (2021)	CTD samples	IVARS	19–21 December 2001 2–6 February 2002 23–24 December 2002 26–29 December 2003 3–6 February 2004 21–24 December 2004 29 January to 1 February 2005 27 December 2005 to 9 January 2006 20 November to 3 December 2006	863815
2	McGillicuddy et al. (2017)	CTD Niskin bottle samples	NBP1201	24 December 2011 to 8 February 2012	511219
3	DiTullio (2015a)	CTD samples	NBP1302	12 February 2013 to 16 March 2013	558908
4	DiTullio (2015b)	Underway collected samples	NBP1302U	12 February 2013 to 16 March 2013	558893
5	DiTullio and Lee (2019)	Niskin Bottle samples	CICLOPS	31 December 2017 to 19 February 2018	778881

Note. Data set abbreviations are used throughout the manuscript. All datasets were obtained from BCO-DMO and are accessible via http://lod.bco-dmo.org/id/dataset/ [Data set ID]. IVARS stands for Interannual Variability in the Antarctic-Ross Sea. NBP stands for Nathaniel B. Palmer, and CICLOPS stands for Cobalamin and Iron Co-Limitation of Phytoplankton Species.

The reanalysis data for PAR, T2M, U10, and V10 were obtained from the ERA-Interim Reanalysis data set (Hersbach et al., 2023) maintained by the European Center for Medium-Range Weather Forecasts (ECMWF, https://www.ecmwf.int/). The reanalysis, which uses the 4DVar data assimilation technique, simulates the wind velocity fields (e.g., U10 and V10) of the Ross Sea with high performance (Coggins et al., 2014). However, there is a difference in the time resolution between the reanalysis (T2M, U10, and V10) data and the modeled (PAR) data. Some variables (T2M, U10, and V10) were provided at 6-hr time intervals, such as 0000, 0600, 1200, and 1800 UTC, and PAR consisted of 12-hr time intervals. All data were converted to daily means to standardize time intervals in the ECMWF reanalysis and modeled data, and the time difference with other variables, such as SIC.

CHL_{REC} was then validated using in situ measurement data from five surveys, retrieved from the Biological and Chemical Oceanography Data Management Office (http://www.bco-dmo.org; Table 2). These include: (1) Interannual Variability in the Antarctic-Ross Sea (IVARS), (2) (3) (4) RVIB Nathaniel B. Palmer (NBP1021, 1302, 1302U), and (5) Cobalamin and Iron Co-Limitation of Phytoplankton Species (CICLOPS). The corresponding locations of these measurements are marked in Figure 1. The data set comprises a total of 216 in situ measurements (75 stations from IVARS, 89 stations from NBP1201, 3 stations from NBP1302, 26 stations from NBP1302U, and 23 stations from CICLOPS) collected at depths of 0 m, 1 m, and 5 m. Only measurements from regions with SIC below 60% and where CHL_{REC} was reconstructed were used for validation. The in situ values were compared with the central point of the CHL_{REC} means over a 3 × 3 pixel window to account for spatial mismatches between the CHL_{SAT} grid and the locations for in situ measurement.

Data noise was filtered prior to RF processing to improve model training performance. This was done by applying the normalized median test to the CHL_{SAT} data set, eliminating any extremely high values (>60 mg m^{-3}) of CHL_{SAT}, considered to be noise (Park et al., 2020; Westerweel & Scarano, 2005; Figure S2 in Supporting Information S1). The filtered CHL_{SAT} data were used as the target variable for reconstruction, and the CHL_{CLIM} was also included as a predictor in the RF model. Due to the distribution of CHL_{SAT} being highly skewed toward low concentration, it posed challenges for model training. Accordingly, we employed a $\log_{10}$ transformation to CHL_{SAT} and CHL_{CLIM} for use as model inputs. Geographical and physical variables were used as predictors (Table 1) and have been validated in a previous study (Park et al., 2020).

Subsequently, the physical variables that affect chlorophyll-a concentration (such as SIC and wind) in each detected regime were further analyzed to determine their individual importance. The total number of non-gap data points was 36,013,371 pixels. The number of pixels used in the training sets for Regime 1 (R1: 1997–2004), Regime 2 (R2: 2005–2016), and Regime 3 (R3: 2017–2019) was 9,003,335,14148,098, and 3,858,572, respectively. Similarly, the validation sets consisted of 3,001,122 for R1, 4,716,048 for R2, and 1,286,195 for R3,

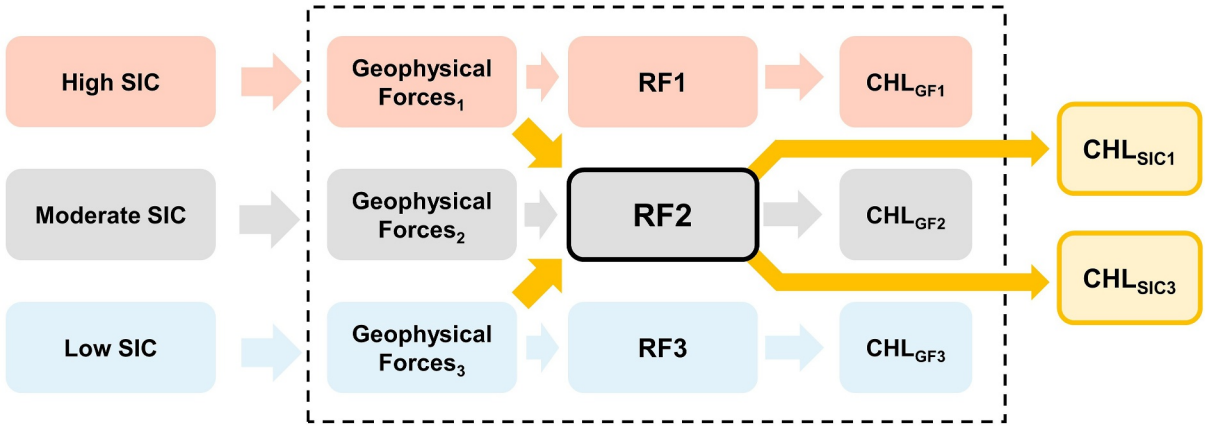

Figure 3. Three different RF models with high, moderate, and low Sea Ice Concentration in each regime. Each regime has corresponding geophysical forces (Geophysical Forces$_1$, Geophysical Forces$_2$, Geophysical Forces$_3$), producing each chlorophyll-a concentration with geophysical forces (CHL_{GF1}, $CHL_{GF2,}$ and CHL_{GF3}), respectively. CHL_{SIC1} and CHL_{SIC2} were produced by Geophysical Forces$_1$ and Geophysical Forces$_3$, respectively.

respectively. To fill CHL_{SAT} gaps caused by dense cloud cover, daily CHL_{SAT} was reconstructed using the RF model for each regime. The data set was split into a 75% training set and a 25% validation set (Figure 2). Based on Figure 2, training and validation accuracies for Regime 1 (R1), Regime 2 (R2), and Regime 3 (R3) were evaluated using R^2, mean squared error (MSE), root mean squared error (RMSE), mean absolute error (MAE), relative mean absolute error, and relative root mean squared error, as shown in Figure 5.

2.3. Quantifying the Phenology of Reconstructed Chlorophyll-A Concentration

In the Ross Sea, rather than diminishing entirely after the primary bloom, chlorophyll-a concentration exhibits a secondary bloom of lower intensity (Smith et al., 2014). Therefore, chlorophyll-a concentration was divided into bloom initiation timing (BIT), bloom peak timing (BPT), and bloom termination timing (BTT) for each regime using the adjusted Gaussian-fitting method (aGFM) based on the CHL_{REC}. The aGFM, which enables the analysis of chlorophyll-a concentration phenology, is defined by the following equation (Park et al., 2019).

$$C(x) = C_0 + h \times e^{\frac{-(x-t_m)^2}{2\sigma^2}} + \frac{d}{1 + e^{\frac{-(x-t_m)}{2\sigma}}} \quad (3)$$

where C_0 is the initial chlorophyll-a concentration, h is the bloom amplitude, x is the time step, t_m is the BPT, σ is the bloom width, and d represents the residual chlorophyll-a concentration. Bloom initiation timing and BTT were calculated as follows.

$$\mathrm{BIT} = t_m - 2\sigma \quad (4)$$

$$\mathrm{BTT} = t_m + 2\sigma \quad (5)$$

2.4. Physical Drivers of Chlorophyll Variability Across Three Sea Ice Regimes

To quantitatively assess the contributions of SIC and geophysical forces (SST, PAR, T2M, U10, and V10) to chlorophyll variability, we implemented the workflow shown in Figure 3. The boxes and arrows illustrate the steps used to estimate chlorophyll-a concentration for each SIC regime—high, moderate, and low—using the corresponding Random Forest models (RF1, RF2, and RF3). The predictors, including geophysical forces (Table 1), were divided into three SICA periods based on the RSI, referred to as Geophysical Forces$_1$, Geophysical Forces$_2$, and Geophysical Forces$_3$, respectively. Each RF model trained on these sets of predictors showed strong performance in estimating chlorophyll-a concentration under the corresponding SIC conditions, and the resulting estimates are referred to as CHL_{GF1}, CHL_{GF2}, and CHL_{GF3}, respectively. To further investigate the role of geophysical drivers, we applied the RF2 model, originally trained under fluctuating SIC conditions, using geophysical predictor inputs from both high and low SIC scenarios (indicated by yellow arrows). Because

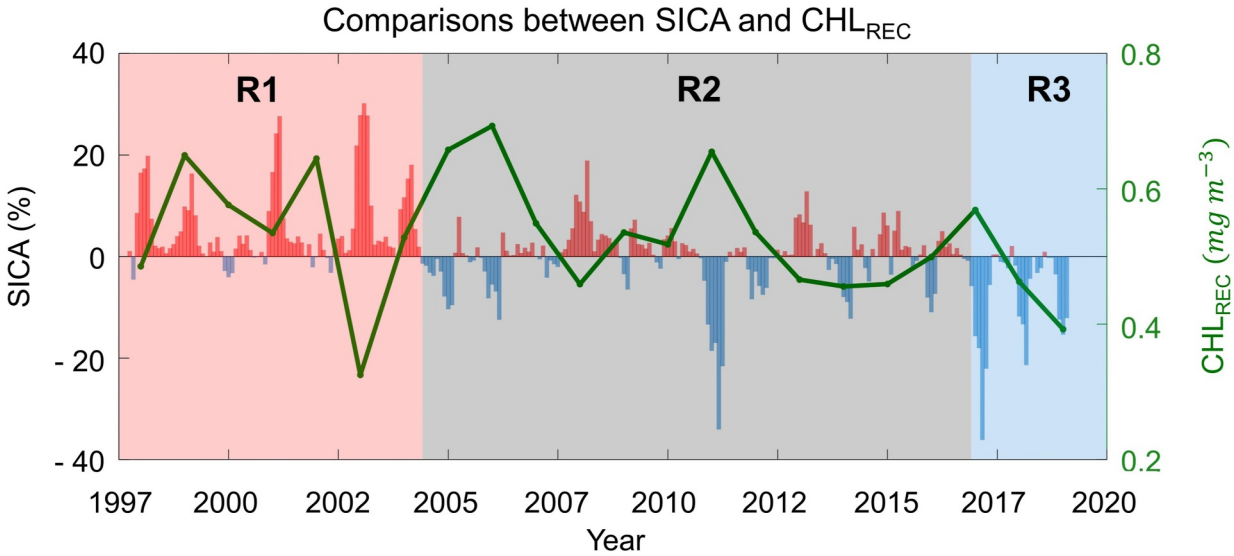

Figure 4. The time series of sea ice concentration anomaly (SICA) distribution is denoted by red and blue bars for the Ross Sea. SICA is divided into three regimes (R1, R2, and R3), derived from the regime shift index (RSI). Mean reconstructed chlorophyll-a concentration (CHL_{REC}) from November to February (green line) is overlaid for comparison.

RF2 is capable of handling varied SIC-related geophysical conditions, the setup allows for an effective comparison. The differences between chlorophyll-a concentration predictions based on geophysical forcing (e.g., CHL_{GF1}) and those based on SIC-specific inputs (e.g., CHL_{SIC1}) provide insights into the dominant drivers of chlorophyll variability. Similarly, comparisons such as CHL_{GF3} versus CHL_{SIC3} help assess the relative influence of geophysical factors versus SIC under low-SIC conditions.

To quantify chlorophyll-a concentration alterations attributed to physical predictors, a partial dependence plot (PDP) was employed. Partial dependence plot is a statistical method that provides a nuanced depiction of how predictors influence the response variable (Friedman, 2001; Greenwell, 2017; Zeng et al., 2017). More specifically, it portrays the relationship between the targeted outcome and selected predictors while controlling for the impact of all other predictors. Partial dependence plot analysis was selected for its ability to quantitatively represent the absolute contribution of each physical variable to CHL_{REC}. Further details on this method can be found in Park et al. (2020). The mean values of each predictor were used to calculate their contributions to CHL_{REC} for each regime.

For a quantitative analysis, we computed the variable importance (VI) of each regime to determine the relationship between model inputs and CHL_{REC}. VI offers a measure of the contribution of an input variable toward the generation of the target data within the RF model and can be calculated by testing the reduction in the model error in each node. After RF training, the total sum of VI is normalized to 1.

3. Results

3.1. Performance of RF for Reconstructing Chlorophyll-A Concentration

Three regimes were classified using RSI on the monthly SICA (Figure 4), with periods defined as follows: R1 (from 1 November 1997–31 May 2004), R2 (from 1 June 2005–31 October 2016), and R3 (from 1 November 2016–28 February 2019).

To fill the missing CHL_{SAT} values under dense clouds, we predicted daily CHL_{SAT} using the RF model for each regime. The predicted CHL_{SAT} from the training and validation data sets was compared with the filtered CHL_{SAT} values for each regime (Figure 5). As a result, the model performance for the training data set showed a high degree of accuracy, with R^2 values of 0.99, 0.99, and 0.99, and RMSE values of 0.20, 0.19, and 0.11 mg m^{-3}, respectively, across the three regimes. Similarly, the validation data set yielded R^2 values of 0.96, 0.97, and 0.98, and RMSE values of 0.43, 0.42, and 0.25 mg m^{-3}, respectively. Among the three regimes, RF3 demonstrated the

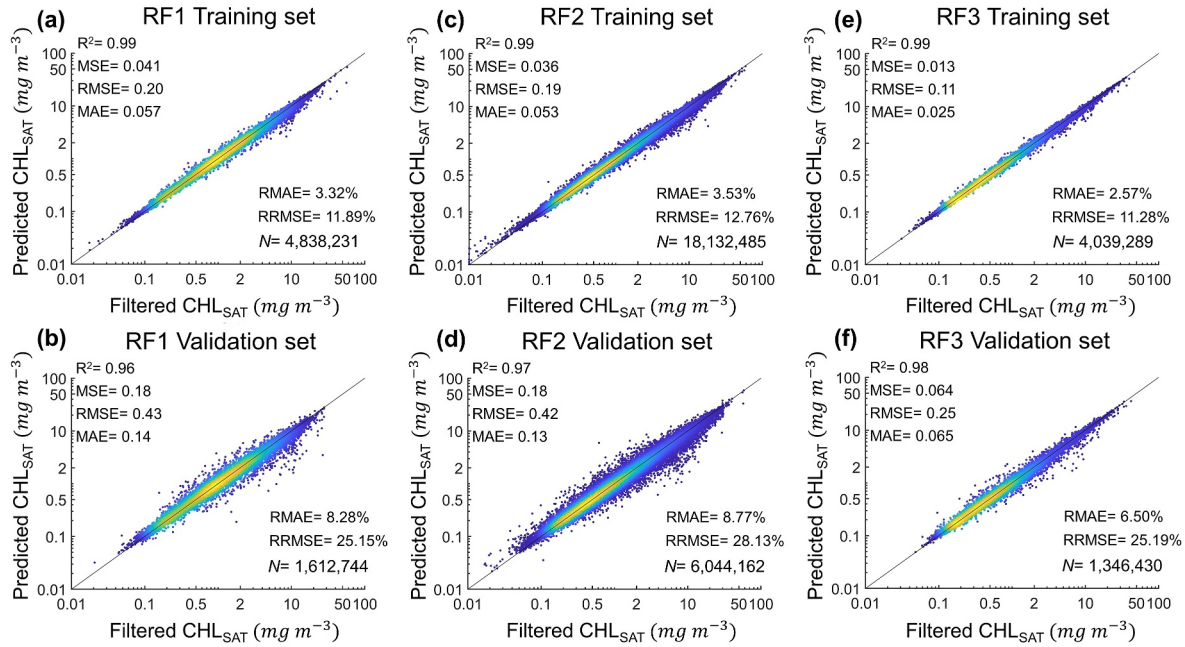

Figure 5. Scatter plots for the comparisons between filtered CHL_{SAT}, which applied the normalized median test, and the predicted CHL_{SAT} with RFs for each regime. RF1, RF2, and RF3 were trained using data from R1, R2, and R3, respectively. Panels (a, c, e) show the training sets for RF1, RF2, and RF3, while panels (b, d, f) show the corresponding validation sets. Statistical metrics and sample size (N) are provided for each case.

best performance. A gap-free CHL_{REC} data set was reconstructed using these RF models. Overall, a slight underestimation was observed when comparing the CHL_{REC} with the 216 in situ data points: the correlation coefficient was 0.8017, and R^2 was approximately 0.64 (Figure S3 in Supporting Information S1).

3.2. Chlorophyll-A Concentration Changes in Response to SIC Regime Shift

Figure 4 shows the monthly SICA and the November–February (NDJF) mean of the CHL_{REC} for the three regimes classified by the RSI. The previously reported inverse relationship between SICA and CHL_{REC} is visible in both R1 and R2, shown in Figure 4 (Criscitiello et al., 2013; Park et al., 2019; Figure S4 in Supporting Information S1). However, CHL_{REC} has been diminishing since 2016, despite the rapidly decreasing trend in SICA.

Once CHL_{SAT} gaps were filled, we analyzed the average CHL_{REC} for each regime on NDJF to examine monthly scale variations (Figure 6). In November, the area with SIC >60% (white regions) was larger in R3 (573,755 km^2) compared to R1 (440,521 km^2) and R2 (357,653 km^2). In contrast, the area with $CHL_{REC} \geq 0.6$ mg m^{-3} was the smallest in R3, showing a decrease of 38.00% and 51.35% compared to R1 and R2, respectively (Table 3). The spatial average of CHL_{REC} in November was highest in R2 and R3, and lowest in R1. In December, R2 exhibited the largest area with $CHL_{REC} \geq 0.6$ mg m^{-3} and the highest average CHL_{REC}, followed by R1, while R3 showed the lowest values. While R1 and R2 showed the highest CHL_{REC} in December despite not having the widest spatial extent, R3 exhibited its peak CHL_{REC} extent and concentration in January. In January, the average CHL_{REC} near Terra Nova Bay was noticeably lower in R3 than in R1 and R2, suggesting a weaker bloom. In February, the CHL_{REC} distribution between Cape Colbeck and the Ross Ice Shelf also showed a significant decrease in R3. The CHL_{REC} patch in R1 had both broader coverage and higher concentrations compared to R3. Specifically, the area with $CHL_{REC} \geq 0.6$ mg m^{-3} decreased by 55.46%, from 377,717 km^2 in R1 to 168,246 km^2 in R3.

Overall, the temporal pattern from November to February indicates that CHL_{REC} and phytoplankton bloom extent were consistently lower in R3 than in R1 and R2, reflecting changes in environmental conditions likely driven by differences in sea ice coverage. Special events, such as the severely limited polynya in 2002/2003 due to excessive iceberg formation (Arrigo & van Dijken, 2003a), may also be considered; excluding this event, however, it is possible that the spatial average CHL_{REC} in R1 was actually higher.

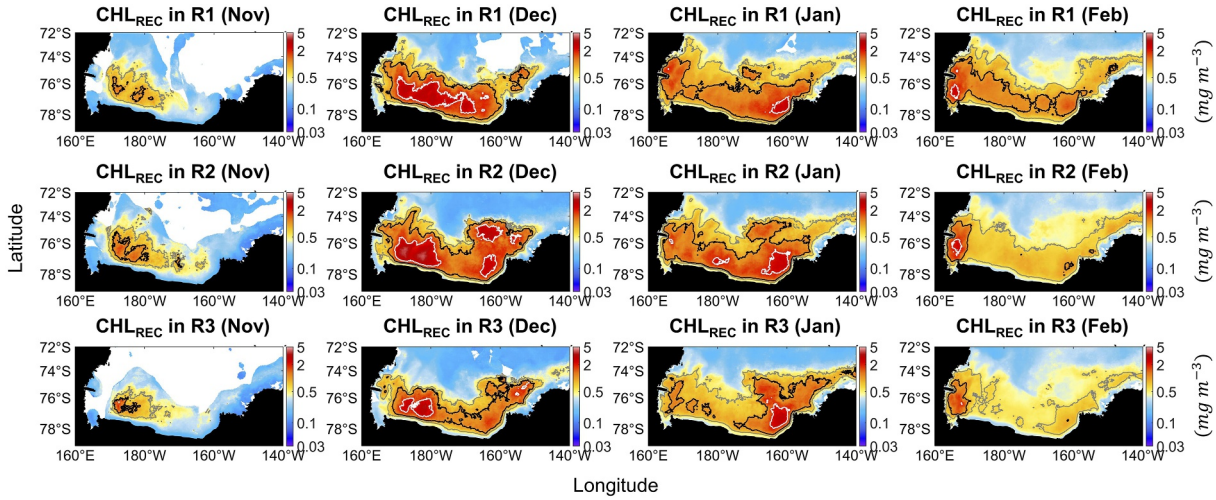

Figure 6. Temporal average of CHL_{REC} in R1, R2, and R3 from the growing season (November to February). Contours indicate mean CHL_{REC} for the 3 mg m^{-3} limit (white), 1 mg m^{-3} limit (black), and 0.6 mg m^{-3} limit (gray), respectively. White areas represent masked regions with Sea Ice Concentration greater than 60%.

To examine phase changes, we fitted CHL_{REC} using the aGFM (Figure 7a), enabling us to infer CHL_{REC} changes in the normal range continuously. We can see that the SIC of the Ross Sea began a gradual decrease lasting from the end of November through February and then began to increase again at the end of February (Figure 7b). Despite SIC starting at the same amount in all three Regimes in November, the melt rate for R3 was approximately twice as fast as that of R1 between December and January (Figure 7b). The dates on which a 50% SIC decrease was observed in the three regimes are 10 January, 22, and 13 December, respectively. The dates with minimum SIC for the three regimes were February 14,19,23, respectively. The time-lag between 50% SIC to the minimum SIC in each regime is 35, 59, and 72 days, respectively, suggesting that sea ice starts to melt earlier from R1 to R3 and continues to melt later. The same difference was also observed in the CHL_{REC} phenology (Figure 7a). In each regime, BIT, BPT, and BTT gradually occurred earlier from R1 to R3. Bloom initiation timing to BPT took 37, 33, and 33 days from R1 to R3, and BPT to BTT took 36, 34, and 33 days from R1 to R3.

3.3. Contributions of SIC and Geophysical Forces to Chlorophyll-A Concentration Changes in Three Regimes

The physical predictors successfully reproduced the spatial patterns of chlorophyll-a concentration across the three SIC regimes. To evaluate the contribution of SIC to changes in CHL_{REC}, we used three RF models, RF1,RF2 and RF3, each trained under distinct SIC conditions: high, moderate, and low, respectively. Notably, RF2 was trained on data from conditions in which SIC alternated between higher and lower values (Figure 4), enabling it to capture chlorophyll-a concentration dynamics under variable SIC influences. As a result, RF2 is particularly useful for examining CHL_{REC}–SIC relationships across fluctuating regimes.

Since all three RF models were trained with the same set of physical predictors but under different SIC regimes, their outputs can be compared to assess the relative impact of SIC on CHL_{REC}. Using the same R1 input data,

Table 3
Area and Spatial Average of CHL_{REC} by Regime and Month

	November		December		January		February	
Regime	$\sum CHL_{REC}$	$\overline{CHL_{REC}}$	$\sum CHL_{REC}$	$\overline{CHL_{REC}}$	$\sum CHL_{REC}$	$\overline{CHL_{REC}}$	$\sum CHL_{REC}$	$\overline{CHL_{REC}}$
R1	78,587	0.34	318,345	0.70	432,725	0.63	377,717	0.57
R2	100,161	0.36	384,045	0.72	440,734	0.67	312,320	0.51
R3	48,724	0.36	293,589	0.52	410,307	0.58	168,246	0.44

Note. $\sum CHL_{REC}$ Indicates the area (km^2) with $CHL_{REC} \geq 0.6$ mg m^{-3}, and $\overline{CHL_{REC}}$ represents the spatial average of CHL_{REC} (mg m^{-3}) in the study area.

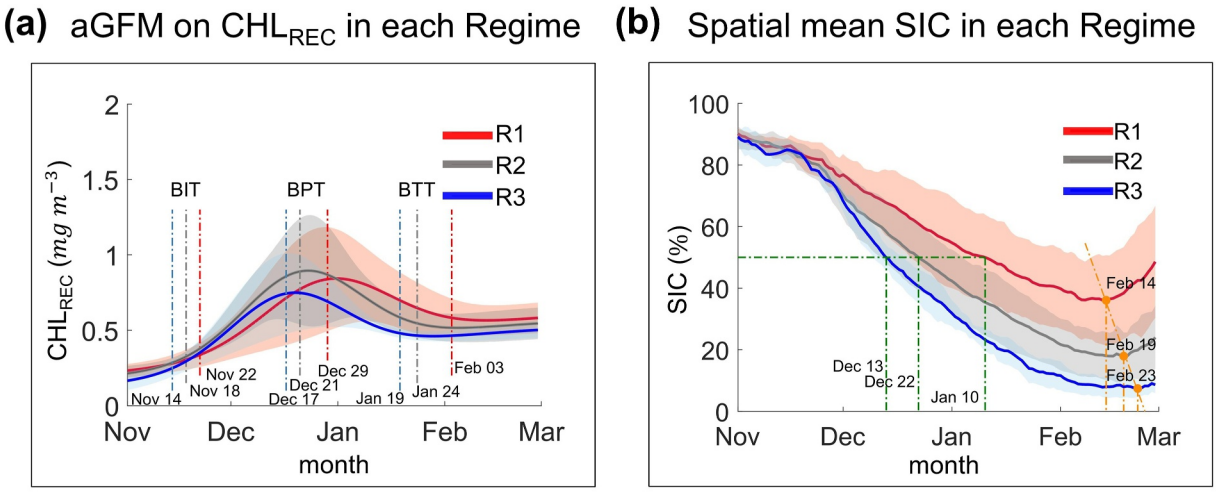

Figure 7. (a) Adjusted Gaussian-fitting method applied to the variation in daily CHL_{REC}. For each regime, three vertical lines (respectively colored: R1, red line; R2, gray line; R3, blue line) are overlaid, representing the bloom initiation timing, bloom peak timing, and bloom termination timing. (b) Mean and standard deviation of Sea Ice Concentration (SIC). The green dashed line indicates the dates when the SIC reached 50%, and the yellow dashed line marks the minimum SIC dates.

CHL_{REC} was estimated under high SIC conditions with RF1 (CHL_{GF1}; Figure 8a) and under moderate SIC conditions with RF2 (CHL_{SIC1}; Figure 8b). Figure 8c shows the difference between CHL_{GF1} and CHL_{SIC1}, with dots indicating areas where the *t*-test results are statistically significant at the 0.05 level. Overall, the mean CHL_{GF1} in R1 is approximately 5 mg m^{-3}, resulting from the combination of geophysical parameters used in this study and potentially influenced by SIC (Figure 8a). Since Figure 8b shows the mean CHL_{SIC1} conditioned on geophysical parameters in R1, the difference between CHL_{GF1} and CHL_{SIC1} shown in Figure 8c represents the effect of SIC, which is approximately 0.5 mg m^{-3}. Thus, during R1, the potential chlorophyll-a concentration change attributable to SIC is approximately 10%, based on the ratio of Figures 8c–8a.

Figure 9 illustrates CHL_{REC} estimates under low SIC conditions using RF3 (CHL_{GF3}; Figure 9a) and under moderate SIC conditions using RF2 (CHL_{SIC3}; Figure 9b), both based on the same R3 input data. The difference map between CHL_{GF3} and CHL_{SIC3} (Figure 9c) shows predominantly negative values, indicating that chlorophyll-a concentration under moderate SIC is generally higher than that under persistently low SIC. Similar to Figures 8c and 8ure 9c shows significantly different regions determined from the *t*-test that meet the 0.05 criterion. As in the chlorophyll-a concentration as described in Figure 8, the mean CHL_{GF3} in R3 is approximately 4.5 mg m^{-3} (Figure 9a), and the differences between CHL_{GF3} and CHL_{SIC3} (Figure 9c) are about 12.5% by the ratio of Figures 9a–9c.

Together, the results from Figures 8 and 9 suggest that variations in chlorophyll-a concentration across different SIC regimes are largely driven by physical predictors (90% and 87.5%) rather than by SIC itself (10% and 12.5%) for R1 and R3, respectively. This suggests that the influence of SIC on chlorophyll-a concentration is secondary to other environmental drivers within the physical predictor set. It is also worth noting that in R2, the contribution of SIC to chlorophyll-a concentration is moderate compared with its role under high and low SIC conditions in R1 and R3. This supports the use of the model to examine the relative contributions of geophysical parameters, as demonstrated.

Overall, the three regimes showed high (R1), moderate (R2), and low (R3) SICA (Figure 4). The average CHL_{REC} and anomalies of the other physical variables for each regime from December to January (DJ), the peak period of phytoplankton blooms, were examined to understand how these changes occurred on a monthly timescale (Figure 10). The spatial relationship between CHL_{REC} and associated geophysical predictors was further examined. In this analysis, the SICA and PAR anomalies showed a gradual decrease from R1 to R3. Conversely, anomalies in SST and T2M show a tendency to increase in R3. During the comparative analysis of the DJ periods, distinct patterns emerge between R1 and R3 in the phases of wind stress curl, the force exerted by the wind on the surface of the water (Figures 10e–10h). Positive (negative) wind stress curl induces surface convergence (divergence) and downwelling (upwelling) via Ekman transport in the Northern Hemisphere (Enriquez &

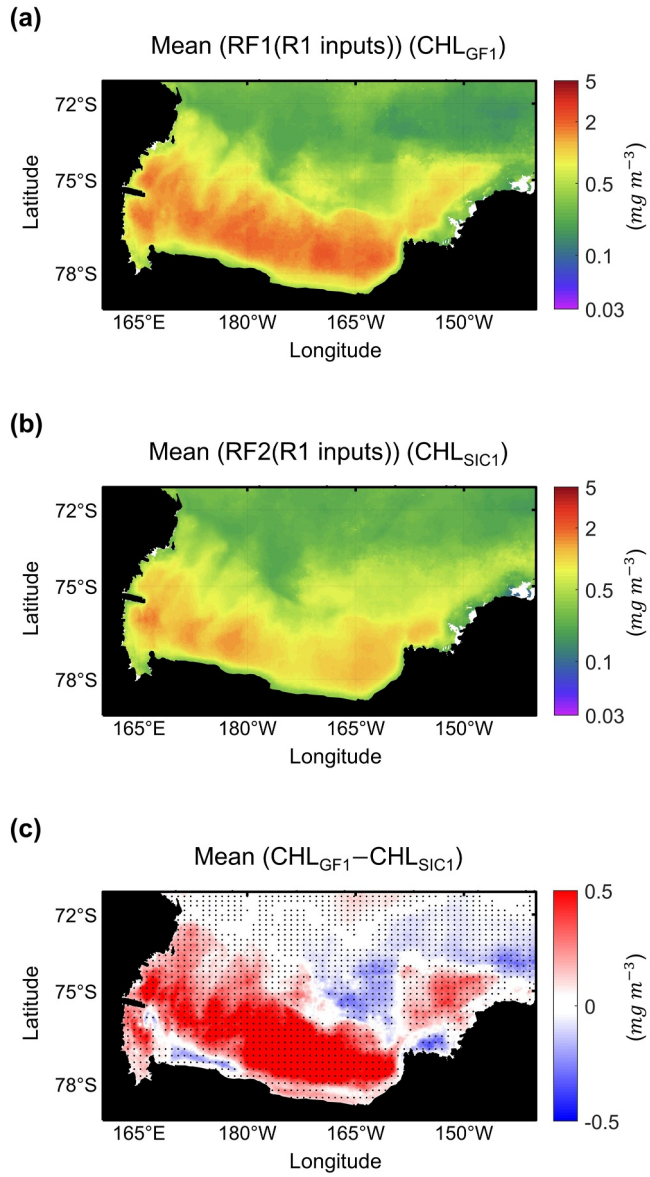

Figure 8. (a) Mean chlorophyll-a concentration from RF1 using R1 inputs (CHL_{GF1}; high Sea Ice Concentration (SIC)); (b) mean chlorophyll-a concentration from RF2 using R1 inputs (CHL_{SIC1}; moderate SIC); and (c) the difference in mean chlorophyll-a concentration between CHL_{GF1} and CHL_{SIC1}. Dots indicate statistically significant regions ($p < 0.05$).

Friehe, 1995; Gill, 1982; Wang et al., 2011), respectively. In the January phase of R1, positive wind stress curls were detected in the proximity of Victoria, with negative wind stress curls forming near Terra Nova Bay and Cape Colbeck (Figure 10f). In contrast, the DJ period of R3 was characterized by strong positive wind stress curls throughout the central Ross Sea and along the coast of the Ross Sea (Figure 10h). Along the Ross Sea coast, R1 could enhance upwelling of nutrient-rich deep water, supporting higher CHL_{REC} levels, whereas the widespread positive curl in R3 may indicate stronger offshore transport that suppresses bloom formation. Moreover, potential feedback may exist, as SIC can influence surface roughness and thus alter wind stress curl patterns, which further complicates the interaction between atmospheric forcing and surface ocean dynamics (Huot et al., 2022).

The mean values of each predictor, depicted by black dashed lines along the *y*-axis (Figure 11), were used to calculate their contributions to CHL_{REC} for each regime. For instance, CHL_{REC} alterations attributed to PAR were 0.95, 0.48, and 0.25 mg m^{-3} for R1, R2, and R3, respectively, corresponding to decreases of 0.47 mg m^{-3} and

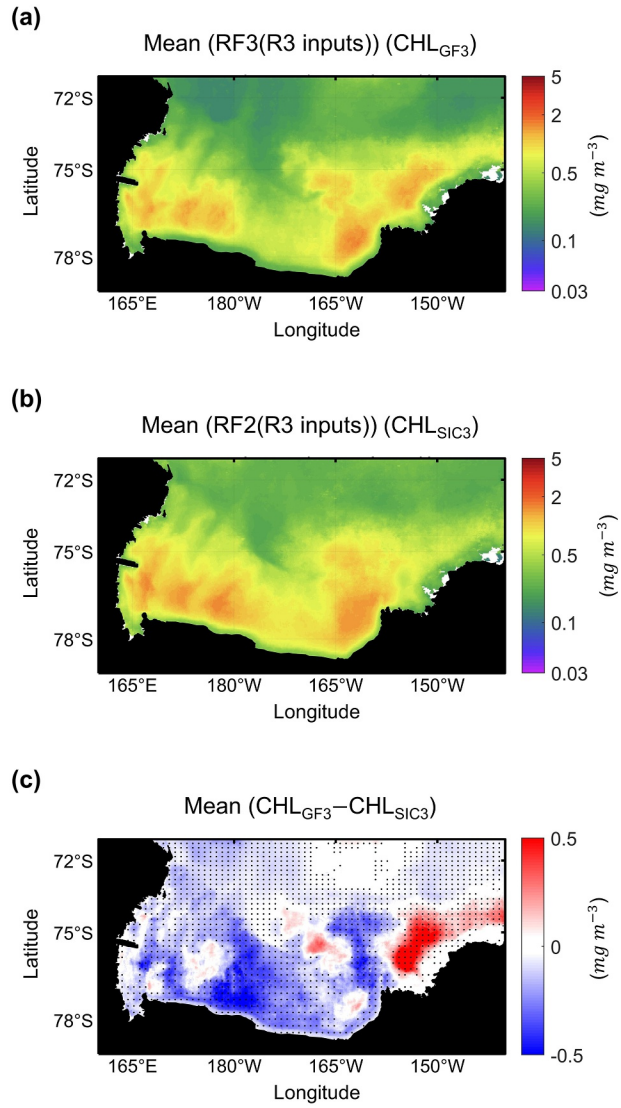

Figure 9. (a) Mean chlorophyll-a concentration from RF3 using R3 inputs (CHL_{GF3}; low Sea Ice Concentration (SIC)); (b) mean chlorophyll-a concentration from RF2 using R3 inputs (CHL_{SIC3}; moderate SIC); and (c) the differences in mean chlorophyll-a concentration between CHL_{GF3} and CHL_{SIC3}. Dots indicate statistically significant regions ($p < 0.05$).

0.23 mg m^{-3} from R1 to R2 and R2 to R3, respectively (Figure 11a). Furthermore, SST (Figure 11b), T2M (Figure 11c), U10 (Figure 11d), and V10 (Figure 11e) are summarized in Table 4.

In addition, regional variations in the environment, triggered by wind and other factors, significantly impact the phenology of chlorophyll-a concentration. Here, we examined VI for all three regimes and obtained different results for each (Figure 11f). In order to examine the model performance, we ran 10 different combinations of different inputs and obtained the standard deviation, which is the brackets in Figure 11f. The contribution of the U10 and V10 to the CHL_{REC} was 1.00% and 1.45% less in R1 than in R3, respectively. In contrast, the contributions of SST and PAR were greater than 2.29% and 0.85%, respectively. For T2M, the contribution was 1.07% higher in R3 than in R1.

4. Discussion and Conclusion

This study evaluates the effect of SIC on phytoplankton bloom phenology in the Ross Sea, using the Ross Sea as a case study for this purpose. We identify the dominant factors responsible for variability in chlorophyll-a concentration across three temporal regimes distinguished by the advancement of sea ice in the Ross Sea, and use

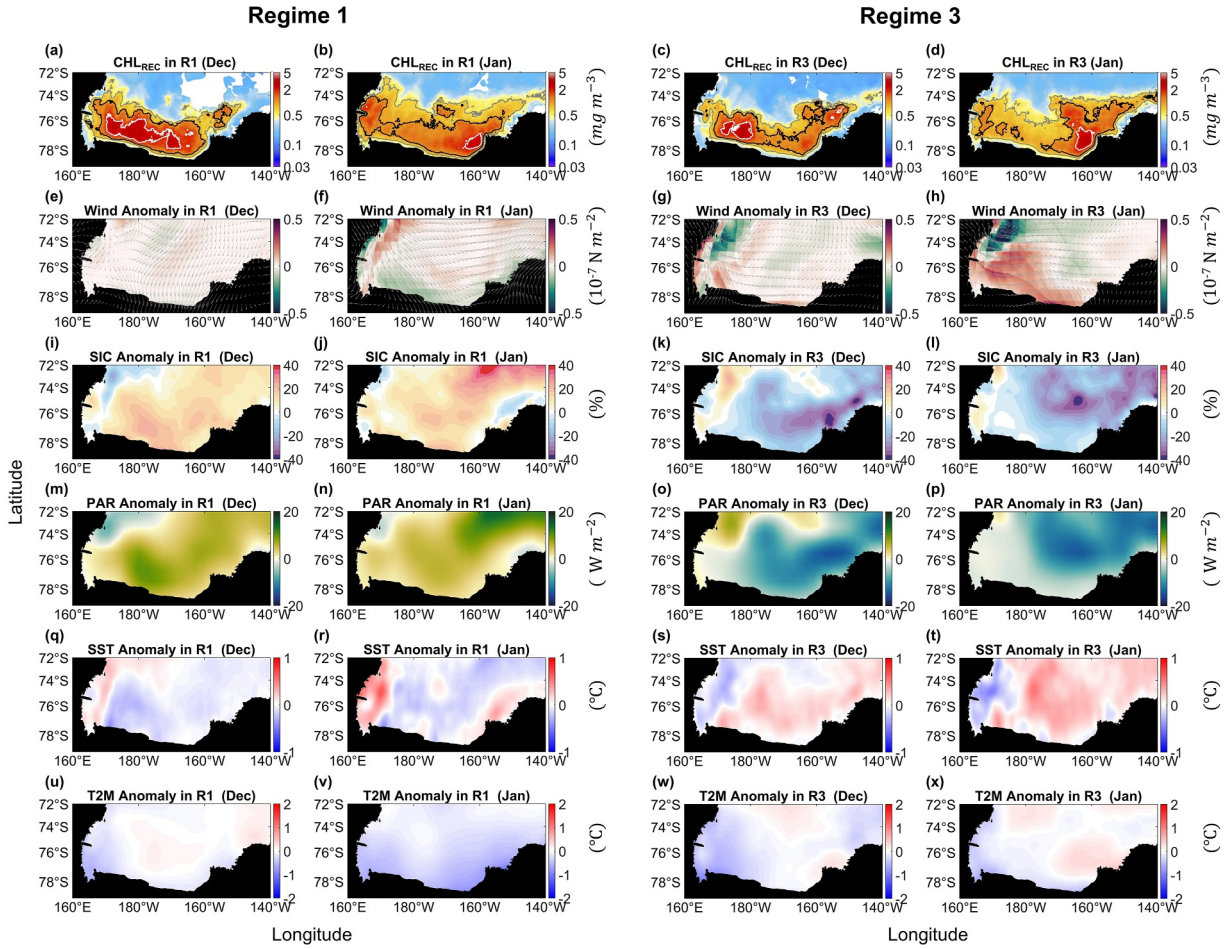

Figure 10. Monthly physical variable distributions of each R1 and R3 used for CHL_{REC} during December and January. (a–d) CHL_{REC} with contours at 3 (white), 1 (black), and 0.6 mg m^{-3} (gray); (e–h) wind stress curl anomaly (background colors) and wind anomaly (gray vectors); (i–l) Sea Ice Concentration anomaly; (m–p) photosynthetically active radiation anomaly; (q–t) Sea surface temperature anomaly; (u)–(x) T2M anomaly. Corresponding distributions for R1–R3 from November to February are shown in Figures S5–S7 in Supporting Information S1.

CHL_{REC} data to analyze phytoplankton bloom phenology within each regime. Each regime was determined by applying the RSI to the Ross Sea SICA distribution. Within these, R1 is characterized by a general increase in SIC, R2 is characterized by a variable SIC, and R3 is characterized by a general decrease in SIC, making the three distinct regimes excellent for comparison.

A detailed discussion of factors such as MLD and stratification, which influence chlorophyll-a dynamics, is essential. However, in this study, MLD was not included as an input variable because model-derived MLD often exhibits substantial biases in the Antarctic owing to limited observations (Sallée et al., 2013; Treguier et al., 2023). To account for their effects indirectly, we constructed the model using variables related to mixing, vertical transport, seasonality, and spatial structure, including wind, DEP, DOY, LON, and LAT. Nevertheless, the omission of variables that directly influence chlorophyll-a concentration, such as MLD and stratification, represents a limitation of this study. Inclusion of these variables in future analyses would likely improve model performance and enable a more direct and quantitative assessment of the effects of upwelling and downwelling on chlorophyll-a concentration, beyond the indirect influence inferred from wind-related processes.

Three regimes were determined based on SICA using RSI, each of which showed positive (R1), fluctuating (R2), and negative (R3) trends. The mechanism linking SIC and chlorophyll-a concentration is as follows: when ice melts, iron supply increases locally, promoting the growth of primary producers in the Ross Sea within newly formed polynyas (Gerringa et al., 2020; McGillicuddy et al., 2015; Portela et al., 2025). In addition, when ice melts, the mixed layer becomes shallower, which increases light penetration and promotes phytoplankton blooms

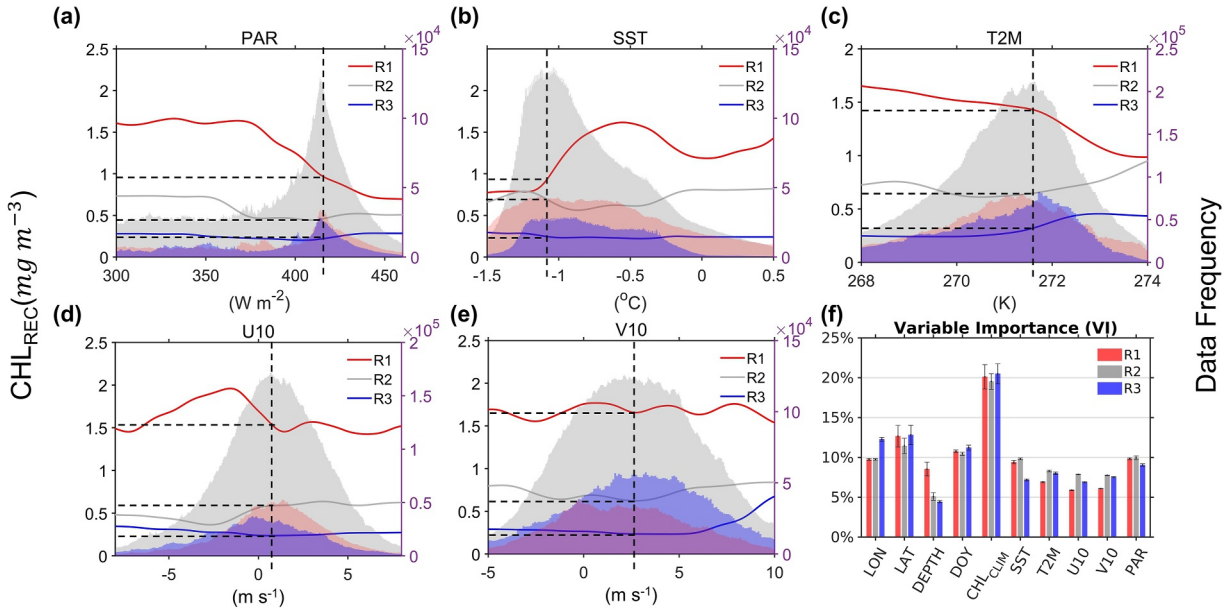

Figure 11. Partial dependence plot of the chlorophyll-a concentration model for physical variables in the order of variable importance (VI): (a) PAR, (b) Sea surface temperature, (c) T2M, (d) U10, and (e) V10. The shaded background represents the data frequency of each predictor. The *y*-axis represents the CHL_{REC} value when the mean values of the other physical variables, excluding the target variable, are used. (f) VI of all variables used as an input of the RF model and each standard deviation. Brackets represent standard deviations from 10 model runs with varying inputs to assess performance stability.

(Smith & Jones, 2015). Specifically, CHL_{REC} was inversely related to SIC in R1 and R2; however, no clear relationship was observed in R3 (Figure 4). While the overall decrease in SIC from R1 to R3 generally supports increased CHL_{REC}, the peak CHL_{REC} in R3 is lower than in R1 and R2. This observation prompted us to examine the relative contributions of both SIC and geophysical predictors. As shown in Figures 8 and 9, geophysical forces appear to have a stronger influence on CHL_{REC} variability than SIC, particularly in R3. These changes can have a significant impact on the Ross Sea because the primary producers distributed along the Ross Sea coast usually show a growth cycle within weeks (Smith et al., 2014). Although we might conclude that decreasing SIC is related to increasing chlorophyll-a concentration in terms of bloom timing, the magnitude of chlorophyll-a concentration is not proportional to SIC; CHL_{REC} in R3 is lower than in R1 and R2. Periods characterized by a positive wind stress curl in the atmospheric dynamics coincide with the phenomenon of surface layer downwelling (Kim et al., 2016, 2017). In January of R3, regions exhibiting strong positive wind stress curl generally corresponded to lower CHL_{REC} relative to R1. This spatial association suggests that enhanced wind-induced downwelling may have suppressed nutrient supply to the euphotic zone, thus reducing phytoplankton biomass. To quantify these differences, PDP analysis revealed that the CHL_{REC} variations induced by U10 and V10 between R1 and R3 were 1.25 mg m^{-3} and 1.5 mg m^{-3}, respectively, which were greater than those caused by other variables (Table 4).

Table 4
Results of Partial Dependence Plot of the CHL_{REC} With Geophysical Predictors Based on RF Models for R1, R2, and R3

PD values at the maximum value of each predictor (mg m^{-3})		Geophysical predictors for CHL_{REC}				
		PAR	SST	T2M	U10	V10
PD of CHL_{REC} at each regime	R1	0.95	0.9	1.4	1.5	1.7
	R2	0.48	0.7	0.75	0.6	0.55
	R3	0.25	0.25	0.25	0.25	0.2
PD differences between regimes	R1—R2	0.47	0.2	0.65	0.9	1.15
	R2—R3	0.23	0.45	0.5	0.35	0.35

This study employs RF modeling to assess the independent contribution of SIC to CHL_{REC} changes and subsequently considers other physical forcing mechanisms. CHL_{REC} changes in response to relatively high SIC in R1 and low SIC in R3 were estimated (Figures 8 and 9). While the contribution of SIC to CHL_{REC} in R1 was approximately 10%, it increased to approximately 12.5% in R3, suggesting that 87.5%–90% of CHL_{REC} variability is driven by other geophysical factors. Furthermore, we estimated that 87.5%–90% of CHL_{REC} variability is explained by geophysical parameters, based on the PDP analysis (Figure 11 and Table 4). PDPs are useful because they show how the RF model relates each input variable to the output, on average, across the data set. This allows us to estimate the relative contribution of each geophysical predictor to changes in chlorophyll-a concentration. As summarized in Table 4, wind speed components were particularly influential in R1, with V10 contributing 1.7 mg m^{-3} and U10 contributing 1.5 mg m^{-3},

followed by near-surface air temperature (T2M, 1.4 mg m^{-3}). In R2, T2M (0.75 mg m^{-3}) and SST (0.7 mg m^{-3}) emerged as the dominant contributors, whereas in R3 the influence of geophysical predictors was more evenly distributed across parameters without a single dominant driver.

We found three major results:

First, Arrigo et al. (2008) and subsequent studies (e.g., Smith et al., 2014) show that earlier sea ice retreat generally leads to an earlier and often more intense bloom. The bloom timing periods were found to gradually shift forward as their distinctive processes accelerated in the transition between R1, R2, and R3.

Second, CHL_{REC} was relatively high in R1, which was the period when the average SIC increased. Notably, CHL_{REC} was relatively low in R3, even when sea ice decreased, unlike R1. Chlorophyll-a concentration changes may therefore be influenced by geophysical parameters (Park et al., 2019) and iron supply due to melting sea ice (Portela et al., 2025).

Finally, geophysical factors accounted for approximately 87.5%–90% of the variability in CHL_{REC} (Figures 8 and 9). According to the VI analysis, the most influential physical drivers of CHL_{REC} variability were PAR, followed by SST, T2M, and wind. Notably, during the R3 period, when the influence of physical variables exceeded that of sea ice, the contribution of PAR was highest. These RF models provide valuable insight into the relative roles of SIC formation and physical environmental parameters in driving the variability in chlorophyll-a concentration.

Conflict of Interest

The authors declare no conflicts of interest relevant to this study.

Data Availability Statement

Sea ice concentration data were obtained from the EUMETSAT Ocean and Sea Ice Satellite Application Facility (OSI SAF) and are available at https://doi.org/10.15770/EUM_SAF_OSI_0014 (OSI SAF, 2022). Chlorophyll-a concentration data were obtained from the GlobColour Chlorophyll-a concentration 1 product suitable for Case-1 waters (version 2018.4), including the Garver-Siegel-Maritorena (GSM) and AVW merged models, available at http://globcolour.info. The SST data were obtained from the NOAA Improvements of the Daily Optimum Interpolation SST (Huang et al., 2021; https://doi.org/10.1175/JCLI-D-20-0166.1). The ERA-Interim Reanalysis data set can be found on Copernicus Climate Change Service (C3S) Climate Data Store (CDS) (https://doi.org/10.24381/cds.adbb2d47) (Hersbach et al., 2023). Global coverage of elevation data was available through GEBCO (GEBCO Compilation Group, 2019; https://doi.org/10.5285/836f016a-33be-6ddc-e053-6c86abc0788e). The in situ measurement data used in this study were obtained from five products conducted in the Ross Sea and were retrieved from the Biological and Chemical Oceanography Data Management Office (http://www.bco-dmo.org). Detailed descriptions of each data set are as follows: (a) CTD samples from the Interannual Variability in the Antarctic-Ross Sea (IVARS) project (Smith, 2021; https://doi.org/10.26008/1912/bco-dmo.863815.2); and (b) CTD Niskin bottle samples from RVIB Nathaniel B. Palmer collected from 24 December 2011–8 February 2012 (McGillicuddy et al., 2017; http://lod.bco-dmo.org/id/dataset/511219); (c) CTD collected samples from RVIB Nathaniel B. Palmer from 12 February 2013–16 March 2013 (DiTullio, 2015a; http://lod.bco-dmo.org/id/dataset/558908); (d) Underway collected samples from the NBP1302 cruise (DiTullio, 2015b; http://lod.bco-dmo.org/id/dataset/558893); and (e) Niskin Bottle samples from Cobalamin and Iron Co-Limitation of Phytoplankton Species (CICLOPS) project (DiTullio & Lee, 2019; https://doi.org/10.1575/1912/bco-dmo.778881.2).

Acknowledgments
This work was supported by the National Research Foundation of Korea (NRF) (Grant: RS-2023-00280650) and Korea Institute of Marine Science & Technology (KIMST) funded by the Ministry of Oceans and Fisheries (Grants: RS-2023-00256330 and RS-2022-KS221661).

References

Arrigo, K. R., & van Dijken, G. L. (2003a). Impact of iceberg C-19 on Ross Sea primary production. *Geophysical Research Letters*, *30*(16). https://doi.org/10.1029/2003GL017721

Arrigo, K. R., & van Dijken, G. L. (2003b). Phytoplankton dynamics within 37 antarctic coastal polynya systems. *Journal of Geophysical Research*, *108*(C8). https://doi.org/10.1029/2002JC001739

Arrigo, K. R., & van Dijken, G. L. (2004). Annual changes in sea-ice, chlorophyll a, and primary production in the Ross Sea, Antarctica. *Deep Sea Research Part II: Topical Studies in Oceanography*, *51*(1–3), 117–138. https://doi.org/10.1016/j.dsr2.2003.04.003

Arrigo, K. R., van Dijken, G. L., & Bushinsky, S. (2008). Primary production in the Southern Ocean, 1997–2006. *Journal of Geophysical Research*, *113*(C8), C08004. https://doi.org/10.1029/2007JC004551

Assmy, P., Fernández-Méndez, M., Duarte, P., Meyer, A., Randelhoff, A., Mundy, C. J., et al. (2017). Leads in Arctic pack ice enable early phytoplankton blooms below snow-covered sea ice. *Scientific Reports*, *7*(1), 40850. https://doi.org/10.1038/srep40850

Atkinson, A., Siegel, V., Pakhomov, E., & Rothery, P. (2004). Long-term decline in krill stock and increase in salps within the Southern Ocean. *Nature*, *432*(7013), 100–103. https://doi.org/10.1038/nature02996

Behera, N., Swain, D., & Sil, S. (2020). Effect of Antarctic sea ice on chlorophyll concentration in the Southern Ocean. *Deep Sea Research Part II: Topical Studies in Oceanography*, *178*, 104853. https://doi.org/10.1016/j.dsr2.2020.104853

Breiman, L. (2001). Random forests. *Machine Learning*, *45*(1), 5–32. https://doi.org/10.1023/A:1010933404324

Chen, S., & Meng, Y. (2022). Phytoplankton blooms expanding further than previously thought in the ross Sea: A remote sensing perspective. *Remote Sensing*, *14*(14), 3263. https://doi.org/10.3390/rs14143263

Clay, S., Peña, A., DeTracey, B., & Devred, E. (2019). Evaluation of satellite-based algorithms to retrieve chlorophyll-a concentration in the Canadian Atlantic and Pacific Oceans. *Remote Sensing*, *11*(22), 2609. https://doi.org/10.3390/rs11222609

Coggins, J. H., McDonald, A. J., & Jolly, B. (2014). Synoptic climatology of the Ross Ice Shelf and Ross Sea region of Antarctica: K-means clustering and validation. *International Journal of Climatology*, *34*(7), 2330–2348. https://doi.org/10.1002/joc.3842

Comiso, J. C., Kwok, R., Martin, S., & Gordon, A. L. (2011). Variability and trends in sea ice extent and ice production in the Ross Sea. *Journal of Geophysical Research*, *116*(C4), C04021. https://doi.org/10.1029/2010JC006391

Criscitiello, A. S., Das, S. B., Evans, M. J., Frey, K. E., Conway, H., Joughin, I., et al. (2013). Ice sheet record of recent sea-ice behavior and polynya variability in the Amundsen Sea, West Antarctica. *Journal of Geophysical Research: Oceans*, *118*(1), 118–130. https://doi.org/10.1029/2012JC008077

DiTullio, G. (2015a). Sample HPLC pigments from RVIB Nathaniel B. Palmer NBP1302 cruise in the Ross Sea during 2013 (TRACERS project) (version 18 May 2015) [Dataset]. *Biological and Chemical Oceanography Data Management Office (BCO-DMO)*. http://lod.bco-dmo.org/id/dataset/558908

DiTullio, G. (2015b). Underway HPLC pigments from the RVIB Nathaniel B. Palmer NBP1302 cruise in the Ross Sea during 2013 [Dataset]. *Biological and Chemical Oceanography Data Management Office (BCO-DMO)*. http://lod.bco-dmo.org/id/dataset/558893

DiTullio, G., & Lee, P. (2019). Algal pigment concentrations measured by HPLC from RVIB Nathaniel B. Palmer cruise in the Ross Sea, Southern Ocean from 2017-2018 (Version 2) [Dataset]. *Biological and Chemical Oceanography Data Management Office (BCO-DMO)*. Version Date 2019-12-24. https://doi.org/10.1575/1912/bco-dmo.778881.2

Enriquez, A. G., & Friehe, C. A. (1995). Effects of wind stress and wind stress curl variability on coastal upwelling. *Journal of Physical Oceanography*, *25*(7), 1651–1671. https://doi.org/10.1175/1520-0485(1995)025<1651:EOWSAW>2.0.CO;2

Fretwell, P. T., Boutet, A., & Ratcliffe, N. (2023). Record low 2022 Antarctic sea ice led to catastrophic breeding failure of emperor penguins. *Communications Earth & Environment*, *4*(1), 273. https://doi.org/10.1038/s43247-023-00927-x

Friedman, J. H. (2001). Greedy function approximation: A gradient boosting machine. *Annals of Statistics*, 1189–1232. http://www.jstor.org/stable/2699986

GEBCO Compilation Group. (2019). GEBCO 2019 Grid [Dataset]. *General Bathymetric Chart of the Oceans (GEBCO)*. https://doi.org/10.5285/836f016a-33be-6ddc-e053-6c86abc0788e

Gerringa, L. J., Alderkamp, A. C., Van Dijken, G., Laan, P., Middag, R., & Arrigo, K. R. (2020). Dissolved trace metals in the Ross Sea. *Frontiers in Marine Science*, *7*, 577098. https://doi.org/10.3389/fmars.2020.577098

Gill, A. E. (1982). *Atmosphere-ocean dynamics* (Vol. 30). Academic Press.

Greenwell, B. M. (2017). Pdp: An R package for constructing partial dependence plots. *RMA Journal*, *9*(1), 421. https://doi.org/10.32614/RJ-2017-016

Hersbach, H., Bell, B., Berrisford, P., Biavati, G., Horányi, A., Muñoz Sabater, J., et al. (2023). ERA5 hourly data on single levels from 1940 to present [Dataset]. *Copernicus Climate Change Service (C3S) Climate Data Store (CDS)*. https://doi.org/10.24381/cds.adbb2d47

Huang, B., Liu, C., Banzon, V., Freeman, E., Graham, G., Hankins, B., et al. (2021). Improvements of the Daily Optimum Interpolation Sea Surface Temperature (DOISST) (version 2.1) [Dataset]. *Journal of Climate*, *34*(8), 2923–2939. https://doi.org/10.1175/JCLI-D-20-0166.1

Huot, P. V., Kittel, C., Fichefet, T., Jourdain, N. C., & Fettweis, X. (2022). Effects of ocean mesoscale eddies on atmosphere–sea ice–ocean interactions off Adélie Land, East Antarctica. *Climate Dynamics*, *59*(1), 41–60. https://doi.org/10.1007/s00382-021-06115-x

Jena, B., & Pillai, A. N. (2020). Satellite observations of unprecedented phytoplankton blooms in the Maud Rise polynya, Southern Ocean. *The Cryosphere*, *14*(4), 1385–1398. https://doi.org/10.5194/tc-14-1385-2020

Kim, C. S., Kim, T. W., Cho, K. H., Ha, H. K., Lee, S., Kim, H. C., & Lee, J. H. (2016). Variability of the Antarctic coastal current in the Amundsen Sea. *Estuarine, Coastal and Shelf Science*, *181*, 123–133. https://doi.org/10.1016/j.ecss.2016.08.004

Kim, T. W., Ha, H. K., Wåhlin, A. K., Lee, S., Kim, C. S., Lee, J. H., & Cho, Y. K. (2017). Is Ekman pumping responsible for the seasonal variation of warm circumpolar deep water in the Amundsen Sea? *Continental Shelf Research*, *132*, 38–48. https://doi.org/10.1016/j.csr.2016.09.005

Li, Y., Ji, R., Jenouvrier, S., Jin, M., & Stroeve, J. (2016). Synchronicity between ice retreat and phytoplankton bloom in circum-antarctic polynyas. *Geophysical Research Letters*, *43*(5), 2086–2093. https://doi.org/10.1002/2016GL067937

Maritorena, S., d'Andon, O. H. F., Mangin, A., & Siegel, D. A. (2010). Merged satellite ocean color data products using a bio-optical model: Characteristics, benefits and issues. *Remote Sensing of Environment*, *114*(8), 1791–1804. https://doi.org/10.1016/j.rse.2010.04.002

Maritorena, S., & Siegel, D. A. (2005). Consistent merging of satellite ocean color data sets using a bio-optical model. *Remote Sensing of Environment*, *94*(4), 429–440. https://doi.org/10.1016/j.rse.2004.08.014

Massom, R. A., & Stammerjohn, S. E. (2010). Antarctic sea ice change and variability–physical and ecological implications. *Polar Science*, *4*(2), 149–186. https://doi.org/10.1016/j.polar.2010.05.001

McGillicuddy, D. J., Dinniman, M., Smith, W. O., Bibby, T., Greenan, B., Sedwick, P. N., et al. (2017). Chemical and biological data from CTD Niskin bottle samples from RVIB Nathaniel B. Palmer NBP1201 in the Ross Sea from 2011-2012 (PRISM-RS project) (Version 2017-05-31) [Dataset]. *Biological and Chemical Oceanography Data Management Office (BCO-DMO)*. http://lod.bco-dmo.org/id/dataset/511219

McGillicuddy, D. J., Jr., Sedwick, P. N., Dinniman, M. S., Arrigo, K. R., Bibby, T. S., Greenan, B. J. W., et al. (2015). Iron supply and demand in an Antarctic shelf ecosystem. *Geophysical Research Letters*, *42*(19), 8088–8097. https://doi.org/10.1002/2015GL065727

O'Reilly, J. E., Maritorena, S., Siegel, D. A., O'Brien, M. C., Toole, D., Mitchell, B. G., et al. (2000). Ocean color chlorophyll a algorithms for SeaWiFS, OC2, and OC4: Version 4. SeaWiFS postlaunch calibration and validation analyses. *Part*, *3*, 9–23.

OSI SAF. (2022). Global sea ice concentration interim climate data record OSI-430-a (Version 3.0) [Dataset]. *EUMETSAT Ocean and Sea Ice Satellite Application Facility*. https://doi.org/10.15770/EUM_SAF_OSI_0014

Park, J., Kim, H. C., Bae, D., & Jo, Y. H. (2020). Data reconstruction for remotely sensed chlorophyll-a concentration in the Ross Sea using ensemble-based machine learning. *Remote Sensing*, *12*(11), 1898. https://doi.org/10.3390/rs12111898

Park, J., Kim, H. C., Jo, Y. H., Kidwell, A., & Hwang, J. (2018). Multi-temporal variation of the Ross Sea Polynya in response to climate forcings. *Polar Research*, *37*(1), 1444891. https://doi.org/10.1080/17518369.2018.1444891

Park, J., Kim, J. H., Kim, H. C., Hwang, J., Jo, Y. H., & Lee, S. H. (2019). Environmental forcings on the remotely sensed phytoplankton bloom phenology in the central Ross Sea polynya. *Journal of Geophysical Research: Oceans*, *124*(8), 5400–5417. https://doi.org/10.1029/2019JC015222

Parkinson, C. L. (2019). A 40-y record reveals gradual Antarctic sea ice increases followed by decreases at rates far exceeding the rates seen in the Arctic. *Proceedings of the National Academy of Sciences*, *116*(29), 14414–14423. https://doi.org/10.1073/pnas.1906556116

Parkinson, C. L., & DiGirolamo, N. E. (2021). Sea ice extents continue to set new records: Arctic, Antarctic, and global results. *Remote Sensing of Environment*, *267*, 112753. https://doi.org/10.1016/j.rse.2021.112753

Portela, E., Meyer, M. G., Heywood, K. J., & Smith, W. O. (2025). Unprecedented summer phytoplankton bloom in the Ross Sea. *Geophysical Research Letters*, *52*(3), e2024GL111264. https://doi.org/10.1029/2024GL111264

Rodionov, S. N. (2004). A sequential algorithm for testing climate regime shifts. *Geophysical Research Letters*, *31*(9). https://doi.org/10.1029/2004GL019448

Saenz, B. T., & Arrigo, K. R. (2014). Annual primary production in Antarctic sea ice during 2005–2006 from a sea ice state estimate. *Journal of Geophysical Research: Oceans*, *119*(6), 3645–3678. https://doi.org/10.1002/2013JC009677

Sallée, J. B., Shuckburgh, E., Bruneau, N., Meijers, A. J., Bracegirdle, T. J., & Wang, Z. (2013). Assessment of Southern Ocean mixed-layer depths in CMIP5 models: Historical bias and forcing response. *Journal of Geophysical Research: Oceans*, *118*(4), 1845–1862. https://doi.org/10.1002/jgrc.20157

Salmon, E., Hofmann, E. E., Dinniman, M. S., & Smith, W. O., Jr. (2020). Evaluation of iron sources in the Ross Sea. *Journal of Marine Systems*, *212*, 103429. https://doi.org/10.1016/j.jmarsys.2020.103429

Smith, W. O. (2021). Compilation of primary productivity measurements collected from 1983-2006 from the Ross Sea (Version 2) [Dataset]. *Biological and Chemical Oceanography Data Management Office (BCO-DMO)*. https://doi.org/10.26008/1912/bco-dmo.863815.2

Smith, W. O., Jr., Ainley, D. G., Arrigo, K. R., & Dinniman, M. S. (2014). The oceanography and ecology of the Ross Sea. *Annual Review of Marine Science*, *6*(1), 469–487. https://doi.org/10.1146/annurev-marine-010213-135114

Smith, W. O., Jr., & Jones, R. M. (2015). Vertical mixing, critical depths, and phytoplankton growth in the Ross Sea. *ICES Journal of Marine Science*, *72*(6), 1952–1960. https://doi.org/10.1093/icesjms/fsu234

Soja-Woźniak, M., Holtrop, T., Woutersen, S., van der Woerd, H. J., Lund-Hansen, L. C., & Huisman, J. (2025). Loss of sea ice alters light spectra for aquatic photosynthesis. *Nature Communications*, *16*(1), 4059. https://doi.org/10.1038/s41467-025-59386-x

Sokolov, S. (2008). Chlorophyll blooms in the Antarctic Zone south of Australia and New Zealand in reference to the Antarctic Circumpolar Current fronts and sea ice forcing. *Journal of Geophysical Research*, *113*(C3). https://doi.org/10.1029/2007JC004329

Thomalla, S. J., Nicholson, S. A., Ryan-Keogh, T. J., & Smith, M. E. (2023). Widespread changes in Southern Ocean phytoplankton blooms linked to climate drivers. *Nature Climate Change*, *13*(9), 975–984. https://doi.org/10.1038/s41558-023-01768-4

Treguier, A. M., de Boyer Montégut, C., Bozec, A., Chassignet, E. P., Fox-Kemper, B., McC. Hogg, A., et al. (2023). The mixed-layer depth in the Ocean Model Intercomparison Project (OMIP): Impact of resolving mesoscale eddies. *Geoscientific Model Development*, *16*(13), 3849–3872. https://doi.org/10.5194/gmd-16-3849-2023

Turner, J., Phillips, T., Marshall, G. J., Hosking, J. S., Pope, J. O., Bracegirdle, T. J., & Deb, P. (2017). Unprecedented springtime retreat of Antarctic sea ice in 2016. *Geophysical Research Letters*, *44*(13), 6868–6875. https://doi.org/10.1002/2017GL073656

Turner, J. S., Munro, D. R., Fay, A., Stammerjohn, S., Kim, H., Schofield, O., & Dierssen, H. (2025). Seasonal variability of surface ocean carbon uptake and Chlorophyll-a concentration in the West Antarctic Peninsula over two decades. *Geophysical Research Letters*, *52*(4), e2024GL112446. https://doi.org/10.1029/2024GL112446

Wang, Q., Kalogiros, J. A., Ramp, S. R., Paduan, J. D., Buzorius, G., & Jonsson, H. (2011). Wind stress curl and coastal upwelling in the area of Monterey Bay observed during AOSN-II. *Journal of Physical Oceanography*, *41*(5), 857–877. https://doi.org/10.1175/2010JPO4305.1

Westerweel, J., & Scarano, F. (2005). Universal outlier detection for PIV data. *Experiments in Fluids*, *39*(6), 1096–1100. https://doi.org/10.1007/s00348-005-0016-6

Yuan, N., Ding, M., Ludescher, J., & Bunde, A. (2017). Increase of the Antarctic sea ice extent is highly significant only in the Ross Sea. *Scientific Reports*, *7*(1), 41096. https://doi.org/10.1038/srep41096

Zeng, C., Yang, L., & Zhu, A. X. (2017). Construction of membership functions for soil mapping using the partial dependence of soil on environmental covariates calculated by random forest. *Soil Science Society of America Journal*, *81*(2), 341–353. https://doi.org/10.2136/sssaj2016.06.0195

Zhan, Y., Luo, Y., Deng, X., Chen, H., Grieneisen, M. L., Shen, X., et al. (2017). Spatiotemporal prediction of continuous daily PM2. 5 concentrations across China using a spatially explicit machine learning algorithm. *Atmospheric Environment*, *155*, 129–139. https://doi.org/10.1016/j.atmosenv.2017.02.023